Journal of Crystal Growth 361 (2012) 85–88

Contents lists available at SciVerse ScienceDirect

Journal of Crystal Growth

journal homepage: www.elsevier.com/locate/jcrysgro

Growth of Zr codoped Er:$LiNbO_3$ and Er/Yb:$LiNbO_3$ single crystal

Yannan Qian [a], Rui Wang [b,*], Biao Wang [a,*], Chao Xu [b], Wei Xu [b], Xiaohong Wu [b], Yanling Xu [b], Lili Xing [b], Chunhui Yang [b]

[a] School of Physics and engineering, Sun Yat-sen University, Guangzhou, 510275, China
[b] Department of Chemistry, Harbin Institute of Technology, Harbin 150001, China

ARTICLE INFO

Article history:
Received 25 February 2012
Received in revised form
5 September 2012
Accepted 11 September 2012
Communicated by: Dr. M. Tischler
Available online 18 September 2012

Keywords:
A1. Doping
A1. Up-conversion
A2. Czochralski method
B1. Lithium niobate

ABSTRACT

Congruent Zr/Er:$LiNbO_3$ and Zr/Er/Yb:$LiNbO_3$ crystals were grown by the Czochralski technique. The structural properties of the grown crystals were confirmed by the powder X-ray diffraction (XRD) patterns. The introduction of Zr^{4+} ions decreased the intensities of the green and red upconversion emissions in Er:$LiNbO_3$ crystal. The green emission resulted from the two- and three-photon processes in Zr/Er:$LiNbO_3$ crystal, and the suppressed cross relaxation processes $^2H_{9/2}+{}^4I_{15/2}\rightarrow{}^2H_{11/2}/{}^4S_{3/2}+{}^4I_{13/2}$ and $^4I_{11/2}+{}^4I_{11/2}\rightarrow{}^4F_{7/2}+{}^4I_{15/2}$ were contribution to the reduced green and red emissions. Zr^{4+} ions doping shortened the lifetime of the $^4S_{3/2}\rightarrow{}^4I_{15/2}$ transition, which was responsible for the decreased green emission in Er:$LiNbO_3$ crystal. In the case of Zr/Er/Yb:$LiNbO_3$ crystal, an enhancement of red emission with respect to the green emission was observed. It was proposed that there was a possible cross relaxation process $^4I_{13/2}+{}^4I_{13/2}\rightarrow{}^4F_{9/2}+{}^4I_{15/2}$ in Zr/Er/Yb:$LiNbO_3$ crystal.

1. Introduction

Lithium niobate ($LiNbO_3$) crystal has garnered much research interest due to its excellent diverse physical properties, such as electro-optical, acousto-optical, ferroelectric, piezoelectric and nonlinear optical properties [1,2]. Inspired by the pioneering concepts of integrated optics (IO), advances in the development of Er-doped $LiNbO_3$ (Er:$LiNbO_3$) waveguide device have been achieved [3,4]. Recently, particular interest has been given to the fundamental investigation on the three-dimensional (3D) Er:$LiNbO_3$ photonic crystals since the refractive index of $LiNbO_3$ (about 2.2) is higher than the required refractive index of 1.9 in 3D photonic bandgap (PBG) materials [5,6]. Furthermore, Er:$LiNbO_3$ crystal could emit the visible green and red upconversion (UC) emissions, covering broad potential application areas, including novel display technologies, optical data storage and undersea communications [7,8].

In order to suppress the optical damage of $LiNbO_3$ crystal, the popular Zr^{4+} ion is selected since its threshold concentration is lower than 2.0 mol%, and its distribution coefficient is close to 1 [9]. The high threshold concentration of the traditional optical damage resistant ions (4.6 mol% for Mg^{2+}, 7.0 mol% for Zn^{2+}, 5 mol% for In^{3+} and 4.0 mol% for Hf^{4+} ion) makes it difficult to grow $LiNbO_3$ crystals of good optical quality [10–13]. Bodziony and Kaczmarek reported that the occupation and the defect structure of an impurity ion in $LiNbO_3$ crystal can be understood by Electron paramagnetic resonance (EPR) [14]. Experimental results suggested that there was the presence of $Yb^{3+}-Yb^{3+}$ pairs in Yb:$LiNbO_3$ host crystal [15,16].

In general, Er:$LiNbO_3$ crystal sensitized by Yb^{3+} ions has been accepted to improve the optical characteristics of Er^{3+} ion under 980 nm excitation [17,18]. This is because Yb^{3+} ion has a large absorption cross section around 980 nm and can efficiently transfer its energy to Er^{3+} ion [19]. In this paper, Zr^{4+} (4 mol%)/Er^{3+} (1 mol%):$LiNbO_3$ and Zr^{4+} (4 mol%)/Er^{3+} (1 mol%)/Yb^{3+} (1 mol%):$LiNbO_3$ crystals were grown by the Czochralski technique. The X-ray diffraction (XRD) was measured to understand the structural properties. The upconversion emission and the time decay spectra were discussed. The pump power dependences and the UC mechanisms in Zr/Er:$LiNbO_3$ and Zr/Er/Yb:$LiNbO_3$ crystals under 980 nm excitation have been studied.

2. Experimental

The congruent (Li/Nb=48.6/51.4) $LiNbO_3$ crystals doped with Zr^{4+} (4 mol%)/Er^{3+} (1 mol%) and Zr^{4+} (4 mol%)/Er^{3+} (1 mol%)/Yb^{3+} (1 mol%) were grown by the Czochralski method along the ferroelectric *c* axis. Er^{3+} (1 mol%):$LiNbO_3$ and Er^{3+}/Yb^{3+} (1 mol%/1 mol%):$LiNbO_3$ crystals were also grown for a comparison. The detailed crystal growth procedures were depicted in Ref. [20]. The grown crystals were polarized at 1200 °C with a current density of 5 mA/cm^2. The four crystals are named as Zr/Er-4/1,

* Corresponding authors.
E-mail addresses: wangrui001@hit.edu.cn (R. Wang), wangbiao@mail.sysu.edu.cn (B. Wang).

0022-0248/$ - see front matter © 2012 Elsevier B.V. All rights reserved.
http://dx.doi.org/10.1016/j.jcrysgro.2012.09.014

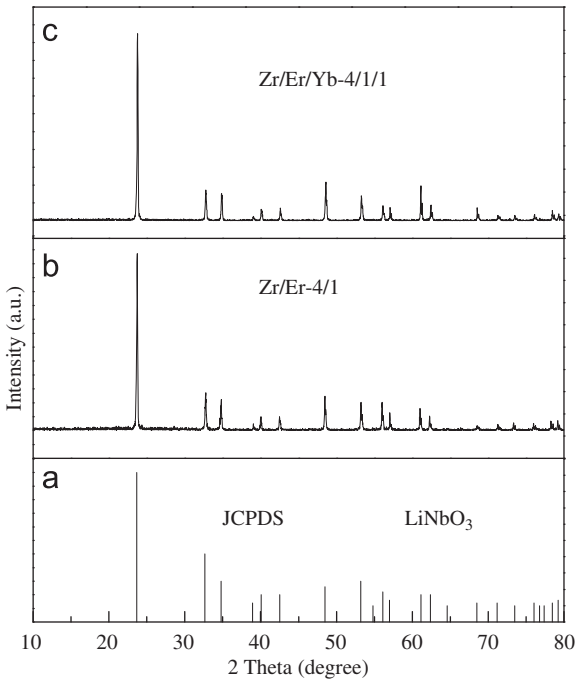

Fig. 1. XRD patterns of Zr/Er-4/1 and Zr/Er/Yb-4/1/1 crystals.

Zr/Er/Yb-4/1/1, Er-1 and Er/Yb-1/1, respectively. The boules were cut into *Y*-cut plates $X \times Y \times Z = 10 \times 2 \times 10\ mm^3$ with carefully polished surfaces.

The powder X-ray diffraction (XRD) patterns were recorded by the D/max-6000 diffraction analysis (SHIMADZU Inc, Japan) with Cu Kα radiation ($\lambda = 0.15406$ nm). The upconversion emission were radiated by the diode laser operating at 980 nm wavelength and recorded by the spectrometer (Bruker optics 500IS/SM) equipped with a semiconductor cooled charge coupled device detector (DV440, Andor). The lifetimes of the $^4S_{3/2} \rightarrow {}^4I_{15/2}$ transition were measured by square-wave modulation of the electric current input to the 980 nm diode laser, and the induced time-resolved curves were recorded by a Yokogawa DLM 2054 digital phosphor oscilloscope.

3. Results and discussions

Fig. 1 shows the powder X-ray diffraction (XRD) patterns of Zr/Er-4/1 and Zr/Er/Yb-4/1/1 crystals. Compared with the pure hexagonal phase (space group:R_{3c}) of stoichiometric $LiNbO_3$ structure (JCPDS no. 85-2456), no new peaks appeared in Zr/Er-4/1 and Zr/Er/Yb-4/1/1 crystals indicate the phase purity of $LiNbO_3$ product. The lattice constants are calculated by the least-squares method, and the unit cell volumes could be obtained by the formula $V = (a^2c) \times \cos 30^\circ$. The lattice constants of ideal $LiNbO_3$ crystal are $a = 0.514829$ nm and $c = 1.38631$ nm [21]. The octahedra sequence of pure $LiNbO_3$ crystal lattice is repeated as [Nb, vacancy, Li], and there are four sites in $LiNbO_3$ crystal, i.e., three octahedral sites (Li^+, Nb^{5+} and cation vacancy) and a tetrahedral interstitial site [22]. Table 1 presents the lattice constants of Zr/Er-4/1 and Zr/Er/Yb-4/1/1 crystals, which are smaller than those of pure $LiNbO_3$ crystal. It has been demonstrated that Er^{3+} and Yb^{3+} ions occupy mostly Li^+ sites [23]. Therefore, based on Li vacancy defect model [24], Er^{3+} and Zr^{4+} ions occupy Li^+ sites, and Er^{2+}_{Li} and Zr^{3+}_{Li} defect groups are formed in Zr/Er:$LiNbO_3$ crystal. Since the polarization abilities of Er^{3+} (45.9) and Zr^{4+} (38.4) are much larger than that of Li^+ (4.2), the lattice constants of Zr/Er-4/1 crystal decrease. The further

Table 1
Lattice constants of standard sample and Zr/Er-4/1 and Zr/Er/Yb-4/1/1 crystals.

Samples	$a=b$ (nm)	c (nm)	V (nm^3)
Pure $LiNbO_3$	0.5148	1.3863	0.31821
Zr/Er-4/1	0.5022	1.3741	0.30013
Zr/Er/Yb-4/1/1	0.5008	1.3753	0.29871

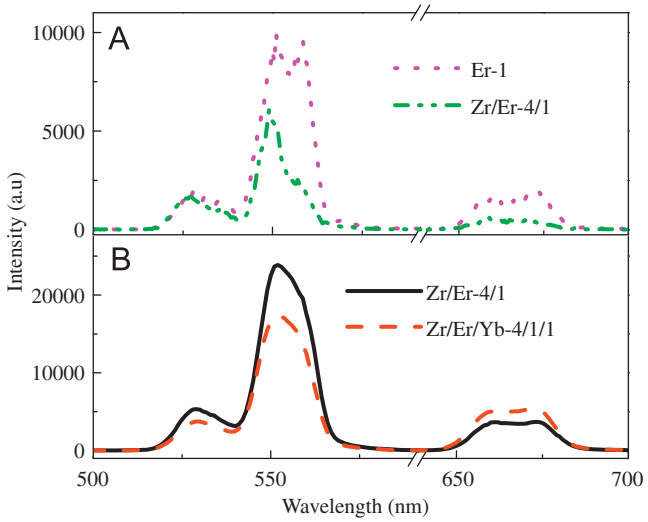

Fig. 2. The green and red UC emission spectra under 980 nm excitation (A) Er-1 and Zr/Er-4/1 crystals; (B) Er/Yb-1/1 and Zr/Er/Yb-4/1/1 crystals.

reduction of lattice constants in Zr/Er/Yb-4/1/1 crystal is attributed to the large polarization ability of Yb^{3+} (50.7). From the view point of the crystallographic considerations, EPR results showed that the Er^{3+}–Er^{3+} pairs locate besides isolated Er^{3+} ions [25].

The UC emission spectra of Er-1 and Zr/Er-4/1 under 980 nm excitation are shown in Fig. 2A. The green UC emissions centered at 525/550 nm are ascribed to the $^2H_{11/2}/{}^4S_{3/2} \rightarrow {}^4I_{15/2}$ transitions of Er^{3+} ion. The red UC emission (660 nm) arises from the $^4F_{9/2} \rightarrow {}^4I_{15/2}$ transition [26]. It is obvious that the intensities of green and red UC emissions decrease with the introduction of the Zr^{4+} ions. Fig. 2B illustrates the UC emission spectra of Er/Yb-1/1 and Zr/Er/Yb-4/1/1 crystals under 980 nm excitation. The Zr^{4+} tridoping leads to a decreased green UC emission and an increase of red UC emission in Zr/Er/Yb:$LiNbO_3$ crystal. The experimental results show that the Zr^{4+} ions result in the different red UC emissions in Er:$LiNbO_3$ and Er/Yb:$LiNbO_3$ crystals.

To better understand the UC mechanism, the intensity of green UC emission is measured as a function of the pump power. The pump power dependences of Zr/Er-4/1 and Zr/Er/Yb-4/1/1 crystals are presented in log–log plot of Fig. 3. In general, for an unsaturated UC process, the required number of photons to populate the upper emitting state can be obtained by the relation $I_f \propto P^n$ [27], where I_f is the fluorescence intensity, P is the pump laser power, and n is the required number of photons. As illustrated in Fig. 3, the n values are equal to 2.5 and 2.1 for Zr/Er-4/1 and Zr/Er/Yb-4/1/1 crystals, respectively. The n value of 2.5 deviates from the expected $n=2$, implying that a three-photon process is involved to populate the green UC emission besides a two-photon process in Zr/Er-4/1 crystal. The $n=2.1$ observed for Zr/Er/Yb-4/1/1 crystal consists with the well known two-photon process to populate the $^4F_{7/2}$ excited state of Er^{3+} ion [28]. The pump power dependences of Er-1 and Er/Yb-1/1 crystals under 980 nm excitation are not investigated here, since the detail studies have been discussed by several groups [29,30].

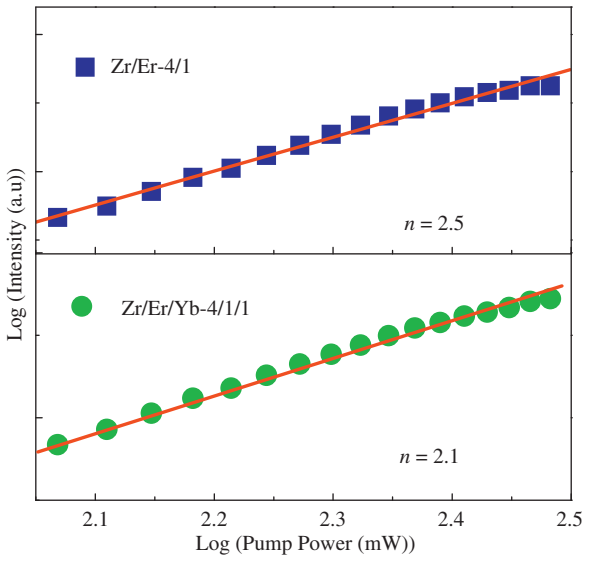

Fig. 3. Pump power dependences for the green UC emission in Zr/Er-4/1 and Zr/Er/Yb-4/1/1 crystals under 980 nm excitation.

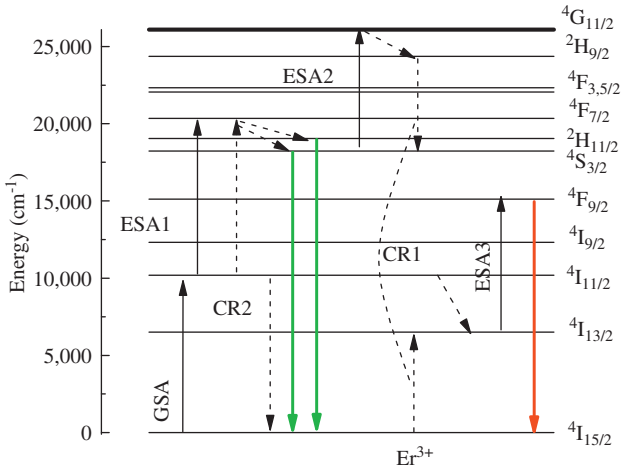

Fig. 4. Energy level diagram of Er^{3+} ion as well as the proposed upconversion mechanism under 980 nm excitation.

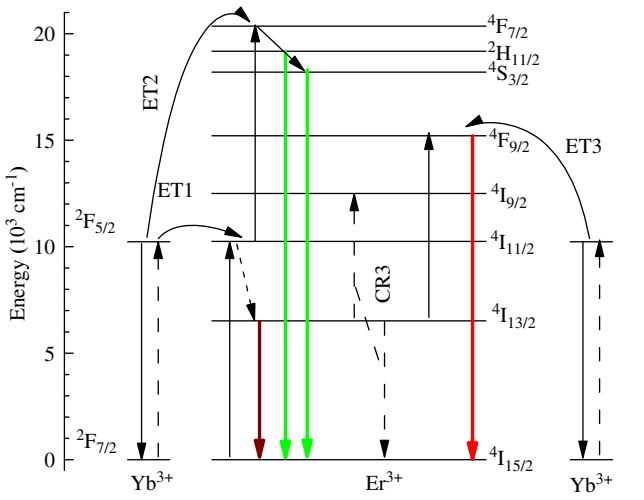

Fig. 5. Energy level diagram of Er^{3+} and Yb^{3+} ions as well as the proposed up-conversion mechanism under 980 nm excitation.

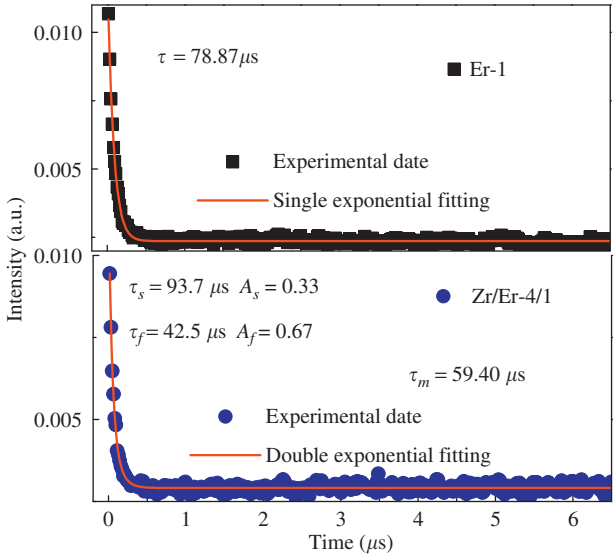

Fig. 6. The fluorescence decays of $^4S_{3/2} \rightarrow {}^4I_{13/2}$ transition in Zr/Er-4/1 and Er-1 crystals.

Fig. 4 displays the energy levels of Er^{3+} ion as well as the proposed UC mechanism in Zr/Er-4/1 crystal. Under 980 nm excitation, Er^{3+} ions at the $^4I_{15/2}$ state are excited to the $^4I_{11/2}$ state via ground state absorption (GSA: $^4I_{15/2}$ + a 980 nm photon $\rightarrow {}^4I_{11/2}$). Then a second 980 nm photon excites the Er^{3+} ion from $^4I_{11/2}$ to $^4F_{7/2}$ state through excited state absorption (ESA1: $^4I_{11/2}$ + a 980 nm photon $\rightarrow {}^4F_{7/2}$). The Er^{3+} ions at the $^4F_{7/2}$ state nonradiatively relax to the $^4S_{3/2}/{}^2H_{11/2}$ states, which subsequently decay radiatively to the $^4I_{15/2}$ state producing the green UC emission. Due to the long lifetime of $^4I_{11/2}$ state, the cross relaxation (CR2) process, $^4I_{11/2} + {}^4I_{11/2} \rightarrow {}^4F_{7/2} + {}^4I_{15/2}$, is contribution to the population of the $^4F_{7/2}$ state. Alternatively, Er^{3+} ions at $^4I_{11/2}$ state would nonradiatively relax to the $^4I_{13/2}$ state, in which Er^{3+} ions are excited to the red emitting $^4F_{9/2}$ state through ESA3: $^4I_{13/2}$ + a 980 nm photon $\rightarrow {}^4F_{9/2}$. The three-photon process is depicted as follows: After GSA and ESA1, a third 980 nm photon promotes the Er^{3+} ion from $^4S_{3/2}$ state to the $^4G_{11/2}$ state by ESA2: $^4S_{3/2}$ + a 980 nm photon $\rightarrow {}^4G_{11/2}$. Since the $^2H_{9/2}$ state can be fed fast via decaying nonradiatively from the $^4G_{11/2}$ state, the CR1 process, $^2H_{9/2} + {}^4I_{15/2} \rightarrow {}^2H_{11/2}/{}^4S_{3/2} + {}^4I_{13/2}$, may occur. It is obvious that CR1 process could increase the population of the $^4S_{3/2}$ and $^4I_{13/2}$ states, and then the intensities of the green and red UC emissions increase. Therefore, the reduced intensities of green and red UC emissions (shown in Fig. 2A) imply that the CR1 and CR2 processes are suppressed by the introduction of Zr^{4+} ions.

The energy level diagrams of Er^{3+} and Yb^{3+} ions as well as the proposed mechanisms in Zr/Er/Yb:$LiNbO_3$ crystal are shown in Fig. 5. Since Yb^{3+} ions have a much large absorption cross section around 980 nm wavelength, the laser excitation of Er^{3+} ions is neglected. Yb^{3+} ions are pumped to the $^2F_{5/2}$ state by absorbing the 980 nm photons, and further transfer their energy to excite Er^{3+} ions from $^4I_{15/2}$ to $^4I_{11/2}$ state via energy transfer (ET1: $^4I_{15/2}$ (Er^{3+}) + $^2F_{5/2}$ (Yb^{3+}) $\rightarrow {}^4I_{11/2}$ (Er^{3+}) + $^2F_{7/2}$ (Yb^{3+})). The $^4F_{7/2}$ state of Er^{3+} ion is populated via ET2: $^4I_{11/2}$ (Er^{3+}) + $^2F_{5/2}$ (Yb^{3+}) $\rightarrow {}^4F_{7/2}$ (Er^{3+}) + $^2F_{7/2}$ (Yb^{3+}). As for the red UC emission, the $^4F_{9/2}$ state is fed from Yb^{3+} ions (ET3: $^4I_{13/2}$ (Er^{3+}) + $^2F_{5/2}$ (Yb^{3+}) $\rightarrow {}^4F_{9/2}$ (Er^{3+}) + $^2F_{7/2}$ (Yb^{3+})). A possible CR3 process ($^4I_{13/2} + {}^4I_{13/2} \rightarrow {}^4F_{9/2} + {}^4I_{15/2}$) may occur between the two neighboring Er^{3+} ions. According to Fig. 5, the CR3 process will lead to an increased population of $^4F_{9/2}$ state, and in turn a depopulation of the $^4I_{13/2}$ state of Er^{3+} ion.

Fig. 6 illustrates the decay curves of $^4S_{3/2} \rightarrow {}^4I_{13/2}$ transition in Er-1 and Zr/Er-4/1 crystals under 980 nm excitation, which are

fitted by single- and double-exponential function, respectively. The single-exponential function is depicted as follow:

$$I(t) = A\exp(-t/\tau) + I_0 \quad (1)$$

where I_0 is the background light intensity, τ is the luminescent lifetime of green UC emission, and A is the weight factors. It can be seen that the luminescent lifetime is 78.87 μs for Er-1 crystal. As for Zr/Er-4/1 crystal, a double-exponential function is used to fit the decay dates [31]:

$$I(t) = I_0 + A_f e^{-t/\tau_f} + A_s e^{-t/\tau_s} \quad (2)$$

where I_0 is the background light intensity, τ_f and A_f are the fast components of the luminescent lifetime and the weight factor, respectively. τ_s and A_s are the slow components of the luminescent lifetime and the weight factor, respectively. The nonexponential behavior of $^4S_{3/2} \rightarrow {}^4I_{13/2}$ transition in Zr/Er-4/1 crystal is because that the $^4S_{3/2}$ states of Er^{3+} ion are populated by ESA or ET. It is well known that A_f and A_s correspond to ESA and ET, respectively. The value ratio of the fast to slow component (A_f/A_s) represents the relative contribution of ESA and ET. The mean decay lifetime (τ_m) could be calculated by the following equation [32]:

$$\tau_m = \int_{t_0}^{\infty} \frac{I(t)}{I_{max}} dt \quad (3)$$

where I_{max} is the maximum of $I(t)[I_{max}=I(t_0=0)]$. As shown in Fig. 6, the fast and slow luminescent lifetimes are τ_f=42.5 μs and τ_s=93.7 μs, respectively; A_f and A_s are equal to 0.67 and 0.33, respectively. A_f/A_s=2 for Zr/Er-4/1 crystal suggests that the $^4S_{3/2}$ state of Er^{3+} ion is mainly populated by ESA process in Zr/Er-4/1 crystal. The mean decay lifetime (τ_m) of Zr/Er-4/1 crystal is 59.4 μs, which is shorter than that of Er-1 crystal. The shortening lifetime caused by Zr^{4+} ion doping means the reduction of green UC emission in Zr/Er-4/1 crystal, in agreement with the experimental results (Fig. 2A).

4. Conclusion

In conclusion, Zr/Er:$LiNbO_3$ and Zr/Er/Yb:$LiNbO_3$ crystals were grown by the Czochralski technique. The two and three-photon processes to populate the green UC emission are observed for Zr/Er:$LiNbO_3$ crystal under 980 nm excitation. The reduced intensity of green UC emission is attributed to the decreasing cross relaxation processes $^2H_{9/2}+{}^4I_{15/2} \rightarrow {}^2H_{11/2}/{}^4S_{3/2}+{}^4I_{13/2}$ and $^4I_{11/2}+{}^4I_{11/2} \rightarrow {}^4F_{7/2}+{}^4I_{15/2}$ in Zr/Er:$LiNbO_3$ crystal. The decay lifetime of $^4S_{3/2} \rightarrow {}^4I_{15/2}$ transition shows a exponential feature in Er:$LiNbO_3$ crystal, and the decay curve in Zr/Er:$LiNbO_3$ crystal is fitted by the double-exponential function. The Zr^{4+} doping shortens the lifetime of green UC emission, which is responsible for the reduction of green UC emission in Er:$LiNbO_3$ crystal. As for Zr/Er/Yb:$LiNbO_3$ crystal, a decreased green and an increased red UC emissions are observed. It is proposed that there is a possible cross relaxation process ($^4I_{13/2}+{}^4I_{13/2} \rightarrow {}^4F_{9/2}+{}^4I_{15/2}$) in Zr/Er/Yb:$LiNbO_3$ crystal.

Acknowledgment

We are grateful to the National Natural Science Foundation of China (Nos. 10732100, 11232015, 11072271 and 10972239) and the Natural Science Foundation of Heilongjiang Province of China (No. B200903). This work is also supported by Prof. ZhiGuo Zhang from Department of Physics of Harbin Institute of Technology.

References

[1] D. Janner, D. Tulli, M. García-Granda, M. Belmonte, V. Pruneri, Laser and Photonics Reviews 3 (2009) 301.
[2] Y. Zhang, Y.H. Xu, M.H. Li, Y.Q. Zhao, Journal of Crystal Growth 242 (2002) 1.
[3] P.R. Hua, D.L. Zhang, Y.M. Cui, Y.F. Wang, E.Y.B. Pun, Crystal Growth and Design 8 (2008) 2125.
[4] E. Cantelar, J.A. Sanz-Garcma, F. Cussó, Journal of Crystal Growth 205 (1999) 196.
[5] N. Susumu, F. Masayuki, A. Takashi, Nature Photonics 1 (2007) 449.
[6] A. Ródenas, G.Y. Zhou, D. Jaque, M. Gu, Advanced Materials 21 (2009) 3526.
[7] F. Auzel, Chemical Reviews 104 (2004) 139.
[8] J.W. Shur, W.S. Yang, S.J. Suh, J.H. Lee, T. Fukuda, D.H. Yoon, Crystal Research and Technology 37 (2002) 353.
[9] Y.F. Kong, S.G. Liu, Y.J. Zhao, H.D. Liu, S.L. Chen, J.J. Xu, Applied Physics Letters 91 (2007) 081908.
[10] N. Iyi, K. Kitamura, Y. Yajima, S. Kimura, Y. Furukawa, M. Sato, Journal of Solid State Chemistry 118 (1995) 148.
[11] T.R. Volk, V.I. Pryalkin, N.M. Rubinina, Optics Letters 15 (1990) 996.
[12] Y.F. Kong, J.K. Wen, H.F. Wang, Applied Physics Letters 66 (1995) 280.
[13] E.P. Kokanyan, L. Razzari, I. Cristiani, V. Degiorgio, J.B. Gruber, Applied Physics Letters 84 (2004) 1880.
[14] T. Bodziony, S.M. Kaczmarek, Physica B: Condensed Matter 400 (2007) 99.
[15] T. Bodziony, S.M. Kaczmarek, Optical Materials 29 (2007) 1440.
[16] G.G. Demirkhanyan, H.G. Demirkhanyan, R.B. Kostanyan, Journal of Contemporary Physics 45 (2010) 215.
[17] E. Cantelar, F. Cussó, Journal of Luminescence 102–103 (2003) 525.
[18] V.G. Babajanyan, R.B. Kostanyan, P.H. Muzhikyan, R.V. Sargsyan, International Conference on Laser Physics (Proceedings of the SPIC), vol. 7998, 2011, p. 799806-1.
[19] Y.J. Huang, H.P. You, Y.H. Song, G. Jia, M. Yang, Y.H. Zheng, L.H. Zhang, K. Liu, Journal of Crystal Growth 312 (2010) 3214.
[20] Y.N. Qian, R. Wang, L.L. Xing, Y.L. Xu, C.H. Yang, X.R. Liu, Crystal Research and Technology 46 (2011) 1137.
[21] T. Bodziony, S.M. Kaczmarek, C. Rudowicz, Physica B: Condensed Matter 403 (2008) 207.
[22] T. Bodziony, S.M. Kaczmarek, J. Hanuza, Journal of Alloys and Compounds 451 (2008) 240.
[23] S.M. Kaczmarek, T. Bodziony, Journal of Non-Crystalline Solids 354 (2008) 4202.
[24] P. Lerner, C. Legras, J.P. Dumas, Journal of Crystal Growth 3–4 (1968) 231.
[25] T. Bodziony, S.M. Kaczmarek, Physica Status Solidi B 245 (2008) 998.
[26] W.S. Yang, H.Y. Lee, D.H. Yoon, Journal of Crystal Growth 244 (2002) 49.
[27] F. Pandozzi, F. Vetrone, J.C. Boyer, R. Naccache, J.A. Capobianco, A. Speghini, M. Bettinelli, Journal of Physical Chemistry B 109 (2005) 17400.
[28] E. Cantelar, F. Cussó, Journal of Physics: Condensed Matter 12 (2000) 521.
[29] P.V. dos Santos, E.A. Gouveia, M.T. de Araujo, A.S. Gouveia-Neto, A.S.B. Sombra, J.A.Medeiros Neto, Applied Physics Letters 74 (1999) 3607.
[30] L.A. Diaz-Torres, O. Meza, D. Solis, P. Salas, E. De la Rosa, Optics and Lasers in Engineering 49 (2011) 703.
[31] H.X. Zhang, C.H. Kam, Y. Zhou, X.Q. Han, S. Buddhudu, Q. Xiang, Y.L. Lam, Y.C. Chan, Applied Physics Letters 77 (2000) 609.
[32] L. Sun, A.H. Li, F.Y. Guo, Q. Lü, Y.H. Xu, L.C. Zhao, Applied Physics Letters 91 (2007) 071914.